
Predicting Deep Neural Network Generalization with Perturbation Response Curves

Yair Schiff
IBM Watson
yair.schiff@ibm.com

Brian Quanz
IBM Research
blquanz@us.ibm.com

Payel Das
IBM Research
daspa@us.ibm.com

Pin-Yu Chen
IBM Research
pin-yu.chen@ibm.com

Abstract

The field of Deep Learning is rich with empirical evidence of human-like performance on a variety of prediction tasks. However, despite these successes, the recent Predicting Generalization in Deep Learning (PGDL) NeurIPS 2020 competition [1] suggests that there is a need for more robust and efficient measures of network generalization. In this work, we propose a new framework for evaluating the generalization capabilities of trained networks. We use perturbation response (PR) curves that capture the accuracy change of a given network as a function of varying levels of training sample perturbation. From these PR curves, we derive novel statistics that capture generalization capability. Specifically, we introduce two new measures for accurately predicting generalization gaps: the Gi-score and Pal-score, that are inspired by the Gini coefficient and Palma ratio (measures of income inequality), that accurately predict generalization gaps. Using our framework applied to *intra* and *inter* class sample mixup, we attain better predictive scores than the current state-of-the-art measures on a majority of tasks in the PGDL competition. In addition, we show that our framework and the proposed statistics can be used to capture to what extent a trained network is invariant to a given parametric input transformation, such as rotation or translation. Therefore, these generalization gap prediction statistics also provide a useful means for selecting the optimal network architectures and hyperparameters that are invariant to a certain perturbation.

1 Introduction

Neural networks have produced state-of-the-art and human-like performance across a variety of tasks. This rapid progress has led to wider-spread adoption and deployment. Given their prevalence and increasing applications, it is important to estimate how well a trained net will generalize. Additionally, specific tasks often require models to be invariant to certain transformations or perturbations of the data. This can be achieved either through data augmentation that changes the underlying statistics of the training sets or through inductive architectural biases, such as translation invariance that is inherent in convolutional neural networks. It is important as well to understand how and when a network has been able to learn task-dependent invariances.

Various attempts at bounding and predicting neural network generalization are well summarized and analyzed in the recent survey [2]. While both theoretical and empirical progress has been made, there remains a gap in the literature for an efficient and intuitive measure that can predict generalization given a trained network and its corresponding data *post hoc*. Aiming to fill this gap, the recent Predicting Generalization in Deep Learning (PGDL) NeurIPS 2020 competition described in [1]

encouraged participants to provide *complexity* measures that would take into account network weights and training data to predict generalization gaps, i.e., the difference between performance on training and test sets.

In this work, we propose a new framework that presents progress towards this goal. Our methodology consists of first building an estimate of how the accuracy of a network changes as a function of varying levels of perturbation present in training samples. To do so, we evaluate a trained network’s accuracy on a subset of the training dataset that has been perturbed to some degree. Using multiple observations of accuracy vs. perturbation magnitude, we develop a perturbation response (PR) curve for each model. From the PR curves, we derive two new measures called the Gi-score and the Pal-score, which compare a given network’s PR curve to that of an idealized network that is unaffected by all perturbation magnitudes. When applying our framework to *inter* and *intra* class Mixup [3] perturbations, we are able to achieve better generalization prediction scores on a majority of the tasks than the current state-of-the-art proposal from the PGDL competition. Because our framework can be applied to any parametric perturbation, we also demonstrate how it can be used to predict the degree to which a network has learned to be invariant to a given perturbation.

2 Related work

The PGDL competition resulted in several proposals of complexity measures that aim to bound and predict neural network generalization gaps. While several submissions build off the work of [4] and rely on margin-based measures, we will focus on those submissions that measure perturbation response, specifically to Mixup, since this is most relevant to our work. Mixup, first introduced in [3], is a novel training paradigm in which training occurs not just on the given training data, but also on linearly interpolated points. Manifold Mixup training extends this idea to interpolation of intermediate network representations [5].

Perhaps most closely related to our work is that of the winning submission, [6]. While [6] presents several proposed complexity measures, the authors explore accuracy on Mixup and Manifold Mixup training sets as potential predictors of generalization gap, and performance on mixed up data is one of the inputs into their winning submission. While this closely resembles our work, in that the authors are using performance on a perturbed dataset, namely a mixed up one, the key difference is that [6] only investigates a network’s response to a single magnitude of interpolation, 0.5. Additionally, we investigate *between*-class interpolation as well, while [6] only interpolates between data points or intermediate representations within a class, not between classes. Our proposed Gi-score and Pal-score therefore provide a much more robust sense for how invariant a network is to this mixing up perturbation and can easily be applied to other perturbations as well.

In the vein of exploring various transformations / perturbations, the second place submission [7] performs various augmentations, such as color saturation, applying Sobel filters, cropping and resizing, and others, and creates a composite penalty score based on how a network performs on these perturbed data points. Our work, in addition to achieving better generalization gap prediction scores, can be thought of as an extension of [7], because as above, rather than looking at a single perturbation level, the Gi-score and Pal-score provide a summary of how a model reacts to a spectrum of parameterized perturbations.

In this work, we also extend our proposed Gi and Pal-scores to predict generalization performance on different invariant data transformations. [8] shows that even for architectures that have inductive biases that should render a network invariant to certain perturbations, in practice these networks are not actually invariant due to how they are trained. This is true even when data augmentation is not carefully employed [8], which highlights the need for our predicting invariance line of work. Unlike works, such as [9], that measure how individual layer and neuron outputs respond to input perturbations, e.g., rotation, translation, and color-jittering, we measure how a network’s overall accuracy responds to these perturbations and compare that to an idealized network that is fully invariant. Consistent prediction on invariant data transformations is a desired property for neural networks [10] and it has been widely used as a data augmentation or regularization tool during training for improving generalization [11].

Our scores are inspired by the Gini coefficient and Palma ratio - most commonly used in economics as measures of income inequality [12–15]. In economics, the Gini coefficient measures income inequality by ordering a population by income and plotting the percentage of the total national income

on the vertical axis vs. the percentage of the population total on the horizontal axis. For an *idealized* economy, wealth distribution lies on a 45° line from the origin, which means each percent of the population holds the same percentage of national wealth. Plotting this distribution for an actual economy allows for the calculation of the Gini coefficient by taking a ratio of the area between the idealized and actual economy wealth distribution curves and dividing by the total area below the idealized economy’s curve. The Palma ratio is also calculated from this plot by taking a ratio of some top $x\%$ of the population’s wealth (area below the actual economy’s curve) divided by that of some bottom $y\%$.

In addition to income inequality, the Gini coefficient has been used in a wide variety of applications in different domains, e.g. measuring biodiversity in ecology [16], quality of life in health [17], and protein selectivity in chemistry [18]. It is also used in machine learning for measuring classification performance, as twice the area between the ROC curve (curve of false positive rate vs. true positive rate for varying classifier threshold) and the diagonal [19, 20] and has also been used as a criteria for feature selection [21]. Our approach is the first to use this metric together with the PR curves for measuring generalization, as well as to use the Pal score in a machine learning setting.

3 Methodology

3.1 Notation

We begin by defining a network for a classification task as $f : \mathbb{R}^d \rightarrow \Delta_k$; that is, a mapping of real input signals x of dimension d to discrete distributions, with Δ_k being the space of all k -simplices. We also define the intermediate layer mappings of a network as $f^{(\ell)} : \mathbb{R}^{d_{\ell-1}} \rightarrow \mathbb{R}^{d_\ell}$, where ℓ refers to a layer’s depth with dimension d_ℓ . The output of each layer is defined as $x^{(\ell)} = f^{(\ell)}(x^{(\ell-1)})$, with inputs defined as $x^{(0)}$. Additionally, let $f_\ell : \mathbb{R}^{d_\ell} \rightarrow \Delta_k$ be the function that maps intermediate representations $x^{(\ell)}$ to the final output of probability distributions over classes. For a dataset \mathcal{D} , consisting of pairs of inputs $x \in \mathbb{R}^d$ and labels $y \in [k]$, a network’s accuracy is defined as $\mathcal{A} = \sum_{x,y \in \mathcal{D}} \mathbb{1}(\max_{i \in [k]} f(x)[i] = y) / |\mathcal{D}|$, i.e. the fraction of samples where the predicted class matches the ground truth label, where $\mathbb{1}(\cdot)$ is an indicator function and $f(x)[i]$ refers to the probability weight of the i^{th} class.

We define perturbations of the network’s representations as $\mathcal{T}_\alpha : \mathbb{R}^{d_\ell} \rightarrow \mathbb{R}^{d_\ell}$, where α controls the magnitude of the perturbation. For example, changing the intensity of an image by α percent can be represented as $\mathcal{T}_\alpha(x^{(0)}) = \alpha x^{(0)}$. To measure a network’s response to a perturbation \mathcal{T}_α applied at the ℓ^{th} layer output, we calculate the accuracy of the network for a sample of the training data on which the perturbation has been applied:

$$\mathcal{A}_\alpha^{(\ell)} = \sum_{x,y \sim \mathcal{D}_{sample}} \mathbb{1}(\max_{i \in [k]} f_\ell(\mathcal{T}_\alpha(x^{(\ell)}))[i] = y) / |\mathcal{D}_{sample}|. \quad (1)$$

The greater the gap $\mathcal{A} - \mathcal{A}_\alpha^{(\ell)}$, the less the network is resilient or invariant to the perturbation \mathcal{T}_α when applied to the ℓ^{th} layer. Perturbations at deeper network layers can be viewed as perturbations in an implicit feature space learned by the network.

3.2 Calculating Perturbation Response curves

To measure a network’s robustness to a perturbation, one could simply choose a fixed α and measure the network’s response. However, a more complete picture is provided by sampling the network’s response to various magnitudes of α . In Figure 1, we show this in practice. For example, letting \mathcal{T}_α refer to image rotation, we vary α from a minimum α_{\min} degree of rotation, to a maximum α_{\max} degree. For each α , we calculate accuracy $\mathcal{A}_\alpha^{(\ell)}$ to measure the network’s response to the perturbation of magnitude α applied at depth ℓ . Plotting $\mathcal{A}_\alpha^{(\ell)}$ on the vertical axis and α on the horizontal axis gives us the PR curves. In Figure 1, we display rotation applied to training images ($\ell = 0$) from the SVHN dataset. This methodology is summarized in Algorithm 1.

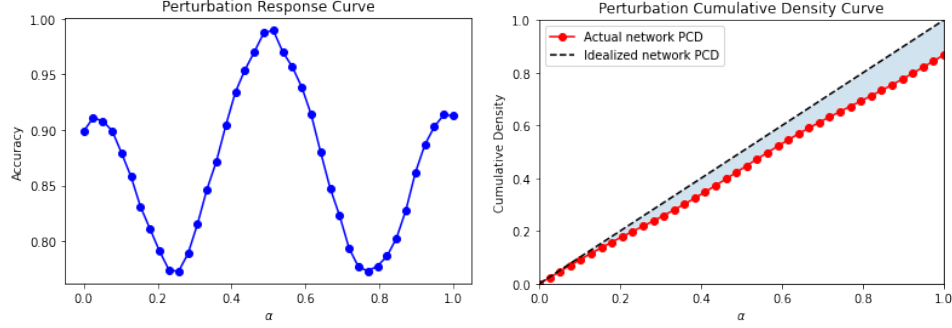


Figure 1: (Left) Sample perturbation response (PR) curve displaying a networks accuracy on 10% of the training data at varying magnitudes of a perturbation. (Right) Sample perturbation cumulative density (PCD) curve comparing the actual network’s cumulative density (red line) to that of an idealized network (dotted black line) with shaded area between the curves, which is used in Gi-score calculations. Pal-score comes from the area below the red curve. These sample plots come from a Resnet [22] model trained on SVHN [23] evaluated with rotation as the parameterized perturbation. α varies from -90° to 90° of rotation and is normalized in the plots to range from 0 to 1.

3.3 Calculating the Gi-score and Pal-score

To extract a single statistic from the PR curves in Figure 1, we draw inspiration from the Gini coefficient and Palma ratio. Namely, we compare a network’s response to varying magnitudes of perturbations with an *idealized* network: one whose accuracy is unaffected by the perturbations. The idealized network therefore has a PR curve that starts and remains at accuracy 1.0.

This comparison is achieved by creating a new graph that plots the cumulative density integral under the PR curves against the magnitudes $\alpha_i \in [\alpha_{\min}, \alpha_{\max}]$: $\int_0^{\alpha_i} \mathcal{A}_\alpha d\alpha$. This produces what we call *perturbation cumulative density* (PCD) curves seen in Figure 1. For the idealized network whose PR is identically equal to 1 for all α , this PCD curve is just the 45° line passing through the origin. Finally, the **Gi-score** (named for the Gini coefficient it draws inspiration from) is calculated by taking a ratio of the area between the idealized network’s PCD curve and that of the actual network and the total area below the idealized network PCD. We summarize this method in Algorithm 2.

The **Pal-score** (named for the Palma ratio it draws inspiration from) calculates the area under the PCD curve and takes a ratio of the area for top 60% of perturbation magnitudes divided by the area for the bottom 10%. This allows us to focus on variations on the upper and lower ends of the perturbation magnitude spectrum, ignoring the middle perturbations that might not vary as widely across networks. Given the similarity to the Gi-score calculation, we defer the pseudocode for the Pal-score to Appendix A.4.

Algorithm 1: Building Perturbation Response (PR) Curve

Inputs: Trained model f ; Dataset \mathcal{D} ; Perturbation \mathcal{T}_α ; Min perturbation magnitude α_{\min} ; Max perturbation magnitude α_{\max} ; Number of perturbation magnitudes to measure n_p ; Layer at which to apply the perturbation ℓ ; number of batches to sample n_b ; batch size b_s

Output: PR Curve: Arrays of regularly spaced perturbation magnitudes ranging from α_{\min} to α_{\max} of length n_p $[\alpha_{\min}, \alpha_{\max}][n_p]$ and accuracy array at each perturbation magnitude of length n_p $\mathcal{A}_\alpha[n_p]$

```

for  $i \leftarrow 0$  to  $n_p - 1$  do
   $\alpha_i \leftarrow [\alpha_{\min}, \alpha_{\max}][i]$ 
  Shuffle  $\mathcal{D}$ 
  for  $k \leftarrow 0$  to  $n_b - 1$  do
     $\mathcal{D}_{sample} \leftarrow \mathcal{D}[kb_s : (k+1)b_s]$  // batch  $k$  of  $\mathcal{D}$ 
     $\mathcal{A}_{\alpha_i}^{(\ell)}[k] \leftarrow$  batch accuracy under perturbation  $\mathcal{T}_{\alpha_i}$  (Equation 1)
   $\mathcal{A}_\alpha[i] \leftarrow \sum_k \mathcal{A}_{\alpha_i}^{(\ell)}[k]/n_b$ 

```

Algorithm 2: Gi-Score computation given PR Curve for a model

Inputs: Arrays of perturbation magnitude $\alpha[n]$ and accuracy $\mathcal{A}_\alpha[n]$ **Output:** Gi-score gi $a_t[0] \leftarrow 0$ // initialize 1st element of trapezoidal areas array with 0**for** $i \leftarrow 0$ **to** $n - 2$ **do** $a_t[i + 1] \leftarrow 0.5(\alpha[i + 1] - \alpha[i])(\mathcal{A}_\alpha[i] + \mathcal{A}_\alpha[i + 1])$ **for** $i \leftarrow 1$ **to** $n - 1$ **do** $a_t[i] \leftarrow a_t[i] + a_t[i - 1]$. // cumulative sum $d[i] = \alpha[i] - a_t[i], \forall i$ $gi = 0$ **for** $i \leftarrow 0$ **to** $n - 2$ **do** $gi \leftarrow gi + 0.5(\alpha[i + 1] - \alpha[i])(d[i] + d[i + 1])$ $gi \leftarrow gi / (0.5\alpha[n - 1]^2)$ // Divide by area under line of equality**return** gi

4 Experiments

4.1 Generalization predictions

To evaluate the extent to which the Gi and Pal scores accurately predict network generalization, we calculate these statistics on the corpus of trained models provided in the PGDL competition [1]. We use the trained networks and their configurations, training data, and “starting kit” code from the competition; all open-sourced and provided under Apache 2.0 license¹. The code includes utilities for loading models and model details, and running scoring. To this base repository, we added our methods for performing different perturbations at different layers, computing PR curves, and computing our proposed Gi and Pal-scores.

4.1.1 Generalization predictions: Experimental setup

The networks from this competition contain the following architectures: VGG [24], Network-in-Network (NiN) [25], and Fully Convolutional [26] (Conv) architectures. The datasets are comprised of CIFAR-10 [27], SVHN [23], CINIC-10 [28], Oxford Flowers [29], Oxford Pets [30], and Fashion MNIST [31]. Note, to our knowledge, these datasets are not known to contain personally identifiable information or offensive content. Although CIFAR-10 and CINIC-100 use images from the problematic ImageNet and Tiny Images [32], they contain manually selected subsets. The list of dataset-model combinations, or tasks, available in the trained model corpus can be seen in the first two rows of Table 1. Across the 8 tasks, there are a total of 550 networks. Each network is trained so that it attains nearly perfect accuracy on the training dataset.

As proposed in [1], the goal is to find a *complexity* measure of networks that is causally informative (predictive) of generalization gaps. To measure this predictive quality, [1] propose a Conditional Mutual Information (CMI) score, which measures how informative the complexity measure is about the network’s generalization given the network’s hyperparameters (i.e., the information contributed by the measure in addition to the network hyperparameters). For full implementation details of this score, please refer to [1] and see Appendix A.2, but roughly, higher values of CMI represent greater capability of a complexity score in predicting generalization gaps.

In our experiments, we let \mathcal{T}_α be defined as an interpolation between two points of either different or the same class: $\mathcal{T}_\alpha(x) = (1 - \alpha)x + \alpha x'$. For *inter*-class interpolation, where x' is a (random) input from a different class than x , we range $\alpha \in [0, 0.5)$. For the *intra*-class setup, where x and x' are drawn from the same class, we include the upper bound of the magnitude: $\alpha \in [0, 0.5]$. While we explored other varieties of perturbation, such as adding Gaussian noise, we found that this interpolation perturbation was most predictive of generalization gaps for the networks and datasets we tested. Both interpolation perturbations that we test (intra- and inter-class) are justifiable for predicting generalization gap. We hypothesize that invariance to interpolation *within* a class should indicate that a network produces similar representations and ultimately the same class maximum

¹<https://github.com/google-research/google-research/tree/master/pgdl>

prediction for inputs and latent representations that are within the same class regions. Invariance to interpolation *between* classes up to 50% should indicate that the network has well separated clusters for representations of different classes and is robust to perturbations moving points away from heavily represented class regions in the data.

4.1.2 Generalization predictions: Results

In Table 1, we present the average CMI scores for all models within a task for our Gi and Pal-scores compared to that of the winning team [6] from the PGDL competition. We also compare our statistic to comparable ones presented in [6] that rely on Mixup and Manifold Mixup accuracy². The winning submission described in [6] uses a combination of a score based on the accuracy of mixed up input data and a clustering quality index of class representations, known as the Davies-Bouldin Index (DBI) [33]. Using the notation introduced in Section 3, the measures from [6] present in Table 1 can be described as follows: Mixup accuracy: $\mathcal{A}_{0.5}^{(0)}$; Manifold Mixup accuracy: $\mathcal{A}_{0.5}^{(1)}$; DBI * Mixup: $DBI * (1 - \mathcal{A}_{0.5}^{(0)})$.

Table 1: Comparison of Conditional Mutual Information scores for various complexity measures across tasks. The highest score within each task among measures that are only based on *mixup* are bolded. For reference, the PGDL winning measure of DBI*Mixup is included in the bottom row. If the best mixup-based score out-performs the winning measure it is also marked with an asterisk. For Gi- an Pal-scores, we indicate whether *Inter* or *Intra* mixup was used for the parametric perturbation along with the depth at which the perturbation was applied in parentheses, with input = 0 and shallowest layer = 1. In the CINIC-10 columns, ‘bn’ stands batch-norm.

	CIFAR-10		SVHN	CINIC-10		Oxford Flowers	Oxford Pets	Fashion MNIST
	<i>VGG</i>	<i>NiN</i>	<i>NiN</i>	<i>Conv w/bn</i>	<i>Conv w/o bn</i>	<i>NiN</i>	<i>NiN</i>	<i>VGG</i>
Gi <i>Inter</i> ($\ell = 0$)	3.12	34.78*	26.86	20.92	6.68	33.35	17.80*	4.49
Gi <i>Inter</i> ($\ell = 1$)	7.69*	24.02	12.25	12.62	8.42	7.39	4.57	16.12*
Pal <i>Inter</i> ($\ell = 0$)	3.17	27.79	22.91	20.94	6.21	29.75	15.96	4.16
Pal <i>Inter</i> ($\ell = 1$)	7.10	13.33	9.65	12.11	7.69	6.27	3.49	14.43
Gi <i>Intra</i> ($\ell = 0$)	0.82	31.73	40.99*	22.80	11.49	40.56	16.80	5.22
Gi <i>Intra</i> ($\ell = 1$)	0.23	16.82	10.98	9.40	12.38	6.85	3.49	5.74
Pal <i>Intra</i> ($\ell = 0$)	0.66	24.64	29.77	24.38	10.93	38.04	15.25	4.93
Pal <i>Intra</i> ($\ell = 1$)	0.45	10.25	14.08	8.80	10.65	5.96	3.02	6.25
Mixup	0.03	14.18	22.75	30.30	19.51*	35.30	9.99	7.75
Manifold Mixup	2.24	2.88	12.11	4.23	4.84	0.03	0.13	0.19
<i>DBI*Mixup</i> ¹	<i>0.00</i>	<i>25.86</i>	<i>32.05</i>	<i>31.79</i>	<i>15.92</i>	<i>43.99</i>	<i>12.59</i>	<i>9.24</i>

These results highlight that the Gi-score and Pal-score perform competitively in predicting generalization gap. Note that some versions of our scores out-perform the mixup approaches used in the PGDL winning approach on the majority of tasks, and even substantially out-perform the DBI*Mixup approach on 5/8 tasks. In addition, we believe that our scores provide a more robust measure for how well a model is able to learn invariances to certain transformations. For example, the Mixup complexity score presented in [6] simply takes a 0.5 interpolation of data points and calculates accuracy of a network on the this mixed up portion of the training set. In contrast, our scores allow us to capture network performance on a spectrum of interpolations, thereby providing a more robust statistic for how invariant a network is to linear data interpolation.

4.1.3 Generalization predictions: Timing and sensitivity analyses

Our proposed PR curve framework is efficiently computed, as it consists of a simple forward pass of a model with computationally efficient perturbations on a subset of the training data. Here we show results of experiments measuring PR curve generation time and CMI scores as a function of number

²Scores come from [6]. For the scores not reported there, we use the code provided by the authors: <https://github.com/parthnatekar/pgdl>

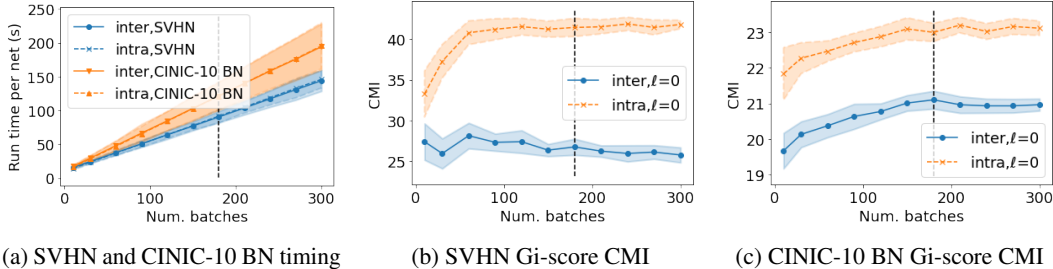


Figure 2: Perturbation response curve generation run times and Conditional Mutual Information score sensitivity results for 2 datasets on input layer ($\ell = 0$). Mean and std. dev. over 20 runs vs. number of batches - 180 batches used in results table (dotted line)

of random batches of the training data, for different perturbation methods and layers for 2 datasets³. For timing analysis on the other tasks, see Appendix A.5. For each batch number experiment, we run 20 random runs and show the mean and standard deviation, to show the sensitivity to the size of the subsample used. Each run is performed with 4 CPUs, 4 GB RAM, and 1 V100 GPU, and batch size 128, submitted as resource-restricted jobs to a cluster with 90+ compute nodes each with 8 GPUs.

As seen in Figure 2, calculations on the number of batches used in our experiments (180) completes well within the PGDL competition 5 minute time limit (although the competition used 1 K80 GPU per score calculation as opposed to the 1 V100 GPU we used, it also used 4 CPUs as we did and 26GB RAM vs. 4 GB we used). We could have even used more batches and still been within the time limit. This illustrates that the proposed method is a good candidate for common use for evaluating network generalization ability, as it does not add significant computational burden.

4.2 Measuring invariance

To test whether our framework could accurately predict the degree to which a network has learned a given invariance, we create our own corpus of trained networks.

4.2.1 Measuring invariance: Experimental setup

We use two model architectures VGG and ResNet [22] and train both architecture types on the CIFAR-10 and SVHN datasets. For the VGG networks, we use varying depths of 11, 13, 16, and 19 hidden layers with and without batch norm. For the ResNet models, we use varying depths of 18, 34, and 50 hidden layers. For all models, we train with batch sizes of either 1024, 2048, or 4096 and learning rates of either $1e^{-4}$ or $1e^{-5}$. All models are trained with Adam optimization and a learning rate scheduler that reduced learning rate on training loss plateaus.

For each combination of model, dataset, batch norm application, batch size, and learning rate we train and test using four different types of parametric perturbations: (1) rotation, (2) horizontal translation, (3) vertical translation, and (4) color jittering. The α_{\min} and α_{\max} for each perturbation are summarized in Table 2. For rotation, the minimum and maximum perturbation values refer to degree of counter-clockwise rotation. Note, that for SVHN, we use a smaller rotation range than for CIFAR-10, since SVHN contain digits, and we would therefore not want even the *idealized* network to be invariant to the full 360° range of rotations. For horizontal translation, the minimum and maximum refer to the amount the image is shifted left or right relative to total image width, with negative values indicating a shift left and positive values indicating a shift right. For vertical translation, the minimum and maximum refer to the amount the image is shifted up or down relative to total image height, with negative values indicating a shift up and positive values indicating a shift down. For color jittering, the minimum and maximum refer to the amount by which brightness, contrast, saturation, and hue are adjusted.

For each perturbation, we train 3 versions of a given hyperparameter combination, one where no data augmentation is used in training, one where partial data augmentation is used in training, and one where full data augmentation is used. Partial data augmentation means that training samples are

³PR curve generation takes the most time, score compute time is negligible in comparison (< 1 millisecond)

Table 2: Perturbation minimum and maximum magnitudes by perturbation type and dataset. Minimum and maximums are displayed in each cell as an ordered pair.

	CIFAR-10	SVHN
Rotation	(-180, 179)	(-90, 90)
Horizontal translation	(-0.5, 0.5)	(-0.5, 0.5)
Vertical translation	(-0.5, 0.5)	(-0.5, 0.5)
Color jittering	(-0.25, 0.25)	(-0.25, 0.25)

randomly perturbed with up to 50% of the perturbation minimum and maximum range. Full data augmentation means that training samples are randomly perturbed within the full range.

For all training paradigms, the test set is randomly augmented with the full perturbation range. Naturally, the models that are also trained with full data augmentation, have better accuracy on the test set. Generalization gap are captured for each model.

Finally, we calculate CMI scores as described in [1] for each architecture type, dataset, and perturbation combination, where the hyperparameters of depth, learning rate, and batch size (and batch norm for VGG networks) are used in the CMI calculation.

4.2.2 Measuring invariance: Results

On each dataset, we calculate CMI scores for each of the two architecture types. We repeat this calculation for each of the four perturbation types. For each dataset, model, and perturbation type, we calculate the CMI score for Gi-scores as well as two baselines: (1) the model’s accuracy on 10% of the training data that is randomly augmented with the full perturbation range and (2) the mean accuracy for all α ’s in the PR curve, i.e., $\frac{1}{n_p} \sum_{\alpha_i=\alpha_{\min}}^{\alpha_{\max}} \mathcal{A}_{\alpha_i}^{(0)}$. We chose these baselines as potentially good indicators of invariance to a specific perturbation, in order to see if our statistic provides added predictive capability. The proposed complexity measures from the PGDL competition, such as Mixup from winning team [6], are less relevant in this context as baselines since they do not directly apply to measuring invariance of the perturbations that we test. We only report results for models that were able to achieve at least 80% accuracy on their respective training sets.

Finally, we note that for the perturbation ranges that we test in this section, the PR curves are not monotonically decreasing as they range from a large magnitude negative perturbation to a large magnitude positive perturbation, see for example Figure 1, which shows the PR curve for a rotation perturbation. Therefore, Pal-scores are omitted from this experiment because they are more applicable in cases where the PR curve is roughly monotonically decreasing.

The results of this experiment are presented in Table 3. With higher CMI scores in almost all scenarios, these results highlight that the Gi-score is more informative than simply seeing how the model performs on a randomly augmented subset of the training data. The results also demonstrate that extracting the Gi-score from PR curves is important, as this statistic is also better at predicting generalization gap than mean accuracy of the PR curve, although this naive alternative is also somewhat informative.

5 Conclusion

In this work, we introduced a general framework, consisting of computing perturbation response (PR) curves, and two novel statistics, inspired by income inequality metrics, which effectively predict network generalization. The Gi and Pal-scores are intuitive and computationally efficient, requiring only several forward passes through a subset of the training data.

Calculating these statistics on the corpus of data made available in [1] showed that our scores applied to linear interpolation between data points have strong performance in predicting a network’s generalization gap. In addition to this predictive capability of generalization, we demonstrated that our framework and the Gi-score provide a useful criterion for evaluating networks and selecting which architecture or hyperparameter configuration is most invariant to a given transformation.

Table 3: Conditional Mutual Information (CMI) scores for all dataset and model combinations across the four perturbations. Each dataset and model is presented in the columns, and the four perturbations are presented separately. For each perturbation, we report CMI for the Gi-score as well as two baselines: (1) the model’s accuracy on 10% of the training data that was randomly augmented with the full perturbation range and (2) the mean accuracy for all α ’s in the PR curve. Within each perturbation we only consider models that attain at least 80% accuracy on their respective datasets, and we report the sample size of models for each setup along the row that indicates which perturbation we are examining. For each perturbation type, we bold the best CMI within a dataset-model combination. For all but two scenarios, the Gi-score provides the best predictive indicator of generalization gap.

	CIFAR-10		SVHN	
	Resnet	VGG	Resnet	VGG
<i>Rotation</i>	($n = 34$)	($n = 93$)	($n = 49$)	($n = 142$)
Acc. on augmented train subset	27.99	16.99	47.24	42.97
Mean acc. on PR curve	27.61	15.61	48.14	44.05
Gi-score	41.54	15.29	54.11	46.11
<i>Horizontal translation</i>	($n = 36$)	($n = 112$)	($n = 50$)	($n = 143$)
Acc. on augmented train subset	41.79	33.48	29.49	24.20
Mean acc. on PR curve	45.03	33.00	29.88	24.28
Gi-score	50.07	34.31	34.56	25.94
<i>Vertical translation</i>	($n = 36$)	($n = 107$)	($n = 49$)	($n = 141$)
Acc. on augmented train subset	26.79	35.68	51.88	50.98
Mean acc. on PR curve	26.55	37.33	52.39	52.22
Gi-score	34.85	39.07	59.02	52.83
<i>Color-jittering</i>	($n = 44$)	($n = 130$)	($n = 49$)	($n = 143$)
Acc. on augmented train subset	35.77	28.44	43.08	30.07
Mean acc. on PR curve	39.12	29.37	43.26	28.67
Gi-score	44.63	30.79	50.08	29.45

Because they rely on comparison with an idealized network that remains unaffected at all magnitudes of a perturbation, our scores are more informative than other baselines that rely on examining how a trained network responds to perturbed data. Specifically, it is interesting to note that our scores provide more informative measures than simply averaging the PR curves or taking the accuracy for random perturbation magnitudes - suggesting our scores may better capture varying effects of different perturbation amounts (perhaps related to discoveries presented in [34] for augmenting training) - future work will explore this hypothesis further. Future work will also demonstrate the usefulness of our statistics on other parametric perturbations and will explore how architectures that are known to be more invariant to certain perturbations, e.g., those described in [10], score in terms of Gi and Pal-scores, when compared to architectures without the inductive biases that contribute to invariance.

Although we provide strong empirical evidence that our framework and Gi and Pal-scores are distinctly informative of network generalization and invariance, currently our approach lacks theoretical underpinning of the performance obtained by these scores. Future work includes deriving theoretical analyses detailing under which conditions our scores correctly identify the best network and correctly rank networks based on generalization, as well as consistency guarantees. Additionally, we plan to evaluate our framework on other tasks and data modalities, such as language models and time series regression.

References

- [1] Y. Jiang, P. Foret, S. Yak, D. M. Roy, H. Mobahi, G. K. Dziugaite, S. Bengio, S. Gunasekar, I. Guyon, and B. Neyshabur, “Neurips 2020 competition: Predicting generalization in deep

- learning,” *arXiv preprint arXiv:2012.07976*, 2020.
- [2] Y. Jiang, B. Neyshabur, H. Mobahi, D. Krishnan, and S. Bengio, “Fantastic generalization measures and where to find them,” in *International Conference on Learning Representations*, 2020. [Online]. Available: <https://openreview.net/forum?id=SJgIPJBFvH>
 - [3] H. Zhang, M. Cisse, Y. N. Dauphin, and D. Lopez-Paz, “mixup: Beyond empirical risk minimization,” *arXiv preprint arXiv:1710.09412*, 2017.
 - [4] Y. Jiang, D. Krishnan, H. Mobahi, and S. Bengio, “Predicting the generalization gap in deep networks with margin distributions,” in *International Conference on Learning Representations*, 2019. [Online]. Available: <https://openreview.net/forum?id=HJIQfnCqKX>
 - [5] V. Verma, A. Lamb, C. Beckham, A. Najafi, I. Mitliagkas, D. Lopez-Paz, and Y. Bengio, “Manifold mixup: Better representations by interpolating hidden states,” in *International Conference on Machine Learning*. PMLR, 2019, pp. 6438–6447.
 - [6] P. Natekar and M. Sharma, “Representation based complexity measures for predicting generalization in deep learning,” 2020.
 - [7] D. Kashyap, N. Subramanyam *et al.*, “Robustness to augmentations as a generalization metric,” *arXiv preprint arXiv:2101.06459*, 2021.
 - [8] A. Azulay and Y. Weiss, “Why do deep convolutional networks generalize so poorly to small image transformations?” *arXiv preprint arXiv:1805.12177*, 2018.
 - [9] I. Goodfellow, H. Lee, Q. Le, A. Saxe, and A. Ng, “Measuring invariances in deep networks,” *Advances in neural information processing systems*, vol. 22, pp. 646–654, 2009.
 - [10] M. M. Bronstein, J. Bruna, T. Cohen, and P. Veličković, “Geometric deep learning: Grids, groups, graphs, geodesics, and gauges,” *arXiv preprint arXiv:2104.13478*, 2021.
 - [11] G. Benton, M. Finzi, P. Izmailov, and A. G. Wilson, “Learning invariances in neural networks,” *Advances in neural information processing systems*, 2020.
 - [12] M. O. Lorenz, “Methods of measuring the concentration of wealth,” *Publications of the American statistical association*, vol. 9, no. 70, pp. 209–219, 1905.
 - [13] A. Cobham and A. Sumner, “Is it all about the tails? the palma measure of income inequality,” *Center for Global Development working paper*, no. 343, 2013.
 - [14] C. Dagum and E. Dagum, “Encyclopedia of statistical sciences,” 2001.
 - [15] P. J. Lambert and J. R. Aronson, “Inequality decomposition analysis and the gini coefficient revisited,” *The Economic Journal*, vol. 103, no. 420, pp. 1221–1227, 1993.
 - [16] L. Wittebolle, M. Marzorati, L. Clement, A. Balloi, D. Daffonchio, K. Heylen, P. De Vos, W. Verstraete, and N. Boon, “Initial community evenness favours functionality under selective stress,” *Nature*, vol. 458, no. 7238, pp. 623–626, 2009.
 - [17] Y. Asada, “Assessment of the health of americans: the average health-related quality of life and its inequality across individuals and groups,” *Population Health Metrics*, vol. 3, no. 1, pp. 1–11, 2005.
 - [18] P. P. Graczyk, “Gini coefficient: a new way to express selectivity of kinase inhibitors against a family of kinases,” *Journal of medicinal chemistry*, vol. 50, no. 23, pp. 5773–5779, 2007.
 - [19] D. J. Hand and R. J. Till, “A simple generalisation of the area under the roc curve for multiple class classification problems,” *Machine learning*, vol. 45, no. 2, pp. 171–186, 2001.
 - [20] M. Bekkar, H. K. Djemaa, and T. A. Alitouche, “Evaluation measures for models assessment over imbalanced data sets,” 2013.

- [21] R. Sanasam, H. Murthy, and T. Gonsalves, "Feature selection for text classification based on gini coefficient of inequality," in *Proceedings of the Fourth International Workshop on Feature Selection in Data Mining*, ser. Proceedings of Machine Learning Research, H. Liu, H. Motoda, R. Setiono, and Z. Zhao, Eds., vol. 10. Hyderabad, India: PMLR, 21 Jun 2010, pp. 76–85. [Online]. Available: <http://proceedings.mlr.press/v10/sanasam10a.html>
- [22] K. He, X. Zhang, S. Ren, and J. Sun, "Deep residual learning for image recognition," in *Proceedings of the IEEE conference on computer vision and pattern recognition*, 2016, pp. 770–778.
- [23] Y. Netzer, T. Wang, A. Coates, A. Bissacco, B. Wu, and A. Y. Ng, "Reading digits in natural images with unsupervised feature learning," 2011.
- [24] K. Simonyan and A. Zisserman, "Very deep convolutional networks for large-scale image recognition," *arXiv preprint arXiv:1409.1556*, 2014.
- [25] M. Lin, Q. Chen, and S. Yan, "Network in network," *arXiv preprint arXiv:1312.4400*, 2013.
- [26] Y. LeCun, Y. Bengio *et al.*, "Convolutional networks for images, speech, and time series," *The handbook of brain theory and neural networks*, vol. 3361, no. 10, p. 1995, 1995.
- [27] A. Krizhevsky, G. Hinton *et al.*, "Learning multiple layers of features from tiny images," 2009.
- [28] L. N. Darlow, E. J. Crowley, A. Antoniou, and A. J. Storkey, "Cinic-10 is not imagenet or cifar-10," *arXiv preprint arXiv:1810.03505*, 2018.
- [29] M.-E. Nilsback and A. Zisserman, "Automated flower classification over a large number of classes," in *2008 Sixth Indian Conference on Computer Vision, Graphics & Image Processing*. IEEE, 2008, pp. 722–729.
- [30] O. M. Parkhi, A. Vedaldi, A. Zisserman, and C. Jawahar, "Cats and dogs," in *2012 IEEE conference on computer vision and pattern recognition*. IEEE, 2012, pp. 3498–3505.
- [31] H. Xiao, K. Rasul, and R. Vollgraf, "Fashion-mnist: a novel image dataset for benchmarking machine learning algorithms," *arXiv preprint arXiv:1708.07747*, 2017.
- [32] V. U. Prabhu and A. Birhane, "Large image datasets: A pyrrhic win for computer vision?" *arXiv preprint arXiv:2006.16923*, 2020.
- [33] D. L. Davies and D. W. Bouldin, "A cluster separation measure," *IEEE transactions on pattern analysis and machine intelligence*, no. 2, pp. 224–227, 1979.
- [34] D. Yin, R. Gontijo Lopes, J. Shlens, E. D. Cubuk, and J. Gilmer, "A fourier perspective on model robustness in computer vision," in *Advances in Neural Information Processing Systems*, H. Wallach, H. Larochelle, A. Beygelzimer, F. d'Alché-Buc, E. Fox, and R. Garnett, Eds., vol. 32. Curran Associates, Inc., 2019. [Online]. Available: <https://proceedings.neurips.cc/paper/2019/file/b05b57f6add810d3b7490866d74c0053-Paper.pdf>
- [35] M. Abadi, A. Agarwal, P. Barham, E. Brevdo, Z. Chen, C. Citro, G. S. Corrado, A. Davis, J. Dean, M. Devin, S. Ghemawat, I. Goodfellow, A. Harp, G. Irving, M. Isard, Y. Jia, R. Jozefowicz, L. Kaiser, M. Kudlur, J. Levenberg, D. Mané, R. Monga, S. Moore, D. Murray, C. Olah, M. Schuster, J. Shlens, B. Steiner, I. Sutskever, K. Talwar, P. Tucker, V. Vanhoucke, V. Vasudevan, F. Viégas, O. Vinyals, P. Warden, M. Wattenberg, M. Wicke, Y. Yu, and X. Zheng, "TensorFlow: Large-scale machine learning on heterogeneous systems," 2015, software available from tensorflow.org. [Online]. Available: <https://www.tensorflow.org/>
- [36] A. Paszke, S. Gross, F. Massa, A. Lerer, J. Bradbury, G. Chanan, T. Killeen, Z. Lin, N. Gimelshein, L. Antiga, A. Desmaison, A. Kopf, E. Yang, Z. DeVito, M. Raison, A. Tejani, S. Chilamkurthy, B. Steiner, L. Fang, J. Bai, and S. Chintala, "Pytorch: An imperative style, high-performance deep learning library," in *Advances in Neural Information Processing Systems 32*, H. Wallach, H. Larochelle, A. Beygelzimer, F. d'Alché-Buc, E. Fox, and R. Garnett, Eds. Curran Associates, Inc., 2019, pp. 8024–8035. [Online]. Available: <http://papers.neurips.cc/paper/9015-pytorch-an-imperative-style-high-performance-deep-learning-library.pdf>

- [37] W. Falcon et al., “Pytorch lightning,” *GitHub*. *Note*: <https://github.com/PyTorchLightning/pytorch-lightning>, vol. 3, 2019.
- [38] A. Paszke, S. Gross, F. Massa, A. Lerer, J. Bradbury, G. Chanan, T. Killeen, Z. Lin, N. Gimelshein, L. Antiga, A. Desmaison, A. Kopf, E. Yang, Z. DeVito, M. Raison, A. Tejani, S. Chilamkurthy, B. Steiner, L. Fang, J. Bai, and S. Chintala, “Pytorch: An imperative style, high-performance deep learning library,” in *Advances in Neural Information Processing Systems 32*, H. Wallach, H. Larochelle, A. Beygelzimer, F. d'Alché-Buc, E. Fox, and R. Garnett, Eds. Curran Associates, Inc., 2019, pp. 8024–8035. [Online]. Available: <http://papers.neurips.cc/paper/9015-pytorch-an-imperative-style-high-performance-deep-learning-library.pdf>

A Appendix

A.1 Assets

For the generalization prediction experiments, we use the data provided by the PGDL competition organizers [1], which is available for download here <https://github.com/google-research/google-research/tree/master/pgdl#wheres-the-data> and is released under the Apache 2.0 license, and corresponding Tensorflow [35] code for loading models, and wrote our perturbation code using Tensorflow as well.

For the measuring invariance experiments, we use the CIFAR-10 [27] dataset, released under the MIT license, and SVHN dataset [23], which does not have a license listed with the dataset. Both datasets were downloaded and split into training and test sets by the `torchvision` module of the PyTorch [36] library.

The packages used in this work and their respective licenses are listed below:

1. PGDL Competition Starter Kit [1]; Apache 2.0
2. PyTorch [36]; BSD
3. PyTorch Lightning [37]; Apache 2.0
4. Tensorflow [35]; Apache 2.0

Completely detailed package and version information is provided in our code (see the "README.md" file for pointers) included in the supplementary materials.

A.2 Calculating Conditional Mutual Information scores

Given it's importance to our analyses, we reproduce the calculation for Conditional Mutual Information (CMI) scores presented in [1] here.

Generalization gap is defined as:

$$g(f, \mathcal{D}) = \sum_{x, y \in \mathcal{D}_{train}} \mathbb{1}(\max_{i \in [k]} f(x)[i] = y) / |\mathcal{D}_{train}| - \sum_{x, y \in \mathcal{D}_{test}} \mathbb{1}(\max_{i \in [k]} f(x)[i] = y) / |\mathcal{D}_{test}|$$

The goal of the PGDL competition was to find a complexity measure μ such that:

$$\text{sgn}(\mu(f, \mathcal{D}_{train}), \mu(f', \mathcal{D}_{train})) = \text{sgn}(g(f, \mathcal{D}), g(f', \mathcal{D}))$$

Let

$$V_g(f, f') = \text{sgn}(g(f, \mathcal{D}), g(f', \mathcal{D}))$$

and

$$V_\mu(f, f') = \text{sgn}(\mu(f, \mathcal{D}_{train}), \mu(f', \mathcal{D}_{train}))$$

Now, we use \mathcal{O} to denote the set of hyperparameters. For example, in Section 4.2, for Resnet models we use $\mathcal{O} = \{\text{depth, learning rate, batch size}\}$ so that $|\mathcal{O}| = 3$. Models can be separated into groups based on their specific value for each hyperparameter. Each group is denoted as \mathcal{O}_k , i.e., the set of models that have hyperparameter configuration k . For each hyperparameter, $\Theta_i \in \mathcal{O}$, $|\Theta_i|$ is the number of possible values that parameter can take on, so that for example, $\Theta_i = \text{Resnet depths of } 18, 34, 50$, we have $|\Theta_i| = 3$. Thus the total number of groups is $\prod_{\Theta_i \in \mathcal{O}} |\Theta_i|$.

If we treat V_g and V_μ as Bernoulli random variables, then we can calculate the probabilities:

$$p(V_g | \mathcal{O}_k), \quad p(V_\mu | \mathcal{O}_k), \quad p(V_g, V_\mu | \mathcal{O}_k)$$

where the probabilities are calculated by counting over models in each group \mathcal{O}_k .

With these probabilities, we can define mutual information between V_g and V_μ :

$$\mathcal{I}(V_g, V_\mu | \mathcal{O}_k) = \sum_{V_g} \sum_{V_\mu} p(V_g, V_\mu | \mathcal{O}_k) \log \left(\frac{p(V_\mu, V_g | \mathcal{O}_k)}{p(V_g | \mathcal{O}_k) p(V_\mu | \mathcal{O}_k)} \right)$$

Each \mathcal{O}_k occurs with the same probability $p_c = 1 / \prod_{\Theta_i \in \mathcal{O}} |\Theta_i|$. Thus, using the same notation abuse as in [1], we have mutual information between V_μ and V_g conditioned on the values of \mathcal{O} :

$$\mathcal{I}(V_g, V_\mu | \mathcal{O}) = \sum_{\mathcal{O}_k} p_c \mathcal{I}(V_g, V_\mu | \mathcal{O}_k)$$

To get values between 0 and 1, we can normalize this conditional mutual information by conditional entropy of generalization, which is defined as:

$$\mathcal{H}(V_g | \mathcal{O}) = \sum_{\mathcal{O}_k} p_c \sum_{V_g} \log(p(V_g | \mathcal{O}_k))$$

So we now have normalized conditional mutual information:

$$\hat{\mathcal{I}}(V_g, V_\mu | \mathcal{O}) = \frac{\mathcal{I}(V_g, V_\mu | \mathcal{O})}{\mathcal{H}(V_g | \mathcal{O})}$$

Finally, the CMI score used in PGDL and presented in the results sections in this work is defined as:

$$\text{CMI}(\mu) = \min_{\mathcal{O}} \hat{\mathcal{I}}(V_g, V_\mu | \mathcal{O})$$

A.3 Algorithm for efficiently computing interpolation PR curves

Here we give more details about how we compute the accuracy under interpolation per batch - for the intra class interpolation. In order to do this efficiently, we compute accuracy per randomly sampled batches with simple operations that can be encoded in a computational graph (e.g., Tensorflow), and then compute the mean accuracy from multiple batch accuracies. Inter class interpolation is performed similarly. In each case, we split the batch into pairs efficiently, by random pairing for inter class interpolation since probability of being from different classes is high, and by sorting by class label and then interleaving the sorted entries to get the pairs, since it is most likely to get pairs of the same class this way. In both cases we throw out any pairs from the batch that do not match (any pairs having the same class for inter class interpolation and any pairs having different class for intra class interpolation). We then compute the accuracy for the batch, and keep track of the effective batch size, to update the total accuracy across all batches.

Algorithm 3: Efficient computation of intra-class interpolation for a batch

Inputs: Sampled batch of data for layer ℓ to perturb $x^{(\ell)}$, y of size n (assume here n is an even number to simplify description), perturbation magnitude $\alpha \in [0, 1]$, and network function $f_{\ell+1}$

Output: Accuracy for batch sample $\mathcal{A}_\alpha^{(\ell)}$

Sort $x^{(\ell)}$, y by class labels y

// Assign every other element, starting with first element

$x_1^{(\ell)} \leftarrow x^{(\ell)}[::2]$

$y_1 \leftarrow y[::2]$

// Assign every other element, starting with second element

$x_2^{(\ell)} \leftarrow x^{(\ell)}[1::2]$

$y_2 \leftarrow y[1::2]$

// Each entry at index i in $x_1^{(\ell)}$ and $x_2^{(\ell)}$, and y_1 and y_2 form pairs

Drop any index i in $x_1^{(\ell)}$, $x_2^{(\ell)}$, y_1 , and y_2 where $y_1[i] \neq y_2[i]$

$x_p^{(\ell)} \leftarrow (1 - \alpha)x_1^{(\ell)} + \alpha x_2^{(\ell)}$ // Get interpolated point

// Compute mean accuracy for interpolated points

$\mathcal{A}_\alpha^{(\ell)} = \sum_j \mathbb{1}(\max_{i \in [k]} f_{\ell+1}(x_p^{(\ell)}[j])[i] = y_1[j]) / |y_1|$

return $\mathcal{A}_\alpha^{(\ell)}$

A.4 Algorithm for computing Pal-scores

In this section, we present the pseudocode for calculating the Pal-score, in Algorithm 4, which is similar to the Gi-score calculation, but with a focus on certain areas of the PCD curve.

Algorithm 4: Pal-Score computation given PR Curve for a model

Inputs: Arrays of perturbation magnitude $\alpha[n]$ and accuracy $\mathcal{A}_\alpha[n]$

Output: Pal-score pal

$a_t[0] \leftarrow 0$ // initialize 1st element of trapezoidal areas array with 0

for $i \leftarrow 0$ to $n - 2$ **do**

$a_t[i + 1] \leftarrow 0.5(\alpha[i + 1] - \alpha[i])(\mathcal{A}_\alpha[i] + \mathcal{A}_\alpha[i + 1])$

$top_idx \leftarrow$ index of 60% of $\alpha[n]$

$bottom_idx \leftarrow$ index of 10% of $\alpha[n]$

$pal \leftarrow a_t[top_idx] / a_t[bottom_idx]$

return pal

A.5 Additional sensitivity analysis

Here we show the timing (Figure 3) and Gi-score CMI (Figure 4) sensitivity results for all datasets for both intra and inter class perturbations, and for both input ($\ell = 0$) and first hidden layer ($\ell = 1$). This analysis is averaged over 20 different runs (each having different random sampling of the full data set per batch) - with mean and standard deviation shown.

The first set of plots shows the timing results for all datasets - shown in Figure 3. We see that for plots, even those with larger number of batches, the time taken to compute our scores is well under the competition time limit - and the longest time dataset (CINIC-10) was already reported in the main paper.

Figure 4 shows the Gi-score CMI sensitivity to number of batches (mean and std. dev.) for all datasets, for both perturb types (inter and intra class) and for both layers (input - layer 0, and layer 1). This confirms the stability of the scores with sufficient sub-sample size (number of batches) and that the number of batches was chosen to be large enough to ensure stable scores in our reported results.

A.6 Measuring invariance: Additional experimental setup information

In this section, we provide additional details about the measuring invariance experiments.

For training the Resnet and VGG networks on CIFAR-10 and SVHN, we rely on the the PyTorch framework [38] and the PyTorch-Lightning wrapper [37]. In order to mimic a real world training paradigm, we split the training sets for both CIFAR-10 and SVHN into 95% training data and 5% validation data.

Each dataset, model, perturbation experiment combination is performed with 1 CPU and 1 V100 GPU.

A.7 Measuring invariance; Additional results

In this section, we include scatter plots of model generalization gap vs. our statistics and the baselines from the measuring invariance experiments.

In each plot, we also include the number of models n , the CMI score, and the Pearson R correlation coefficient. Results are displayed in Figures 5, 6, 7, and 8. Note that, interestingly, correlation and visual inspection do not always completely equate with CMI scores, as CMI specifically measures information provided by the complexity measure beyond what is known given the network hyper-parameters / settings itself (that the score is conditioned on). So, in particular, when the factors conditioned on correlate with generalization gap, the differentiating contribution of the complexity measure itself may not be as easily observable, and the CMI score is needed to fully elucidate the complexity measures' distinct predictive / informative capabilities. We observe that our approach is best able to distinguish the different training condition groups and correlates most strongly with generalization gap, especially when augmented training is not applied so models are less likely to be

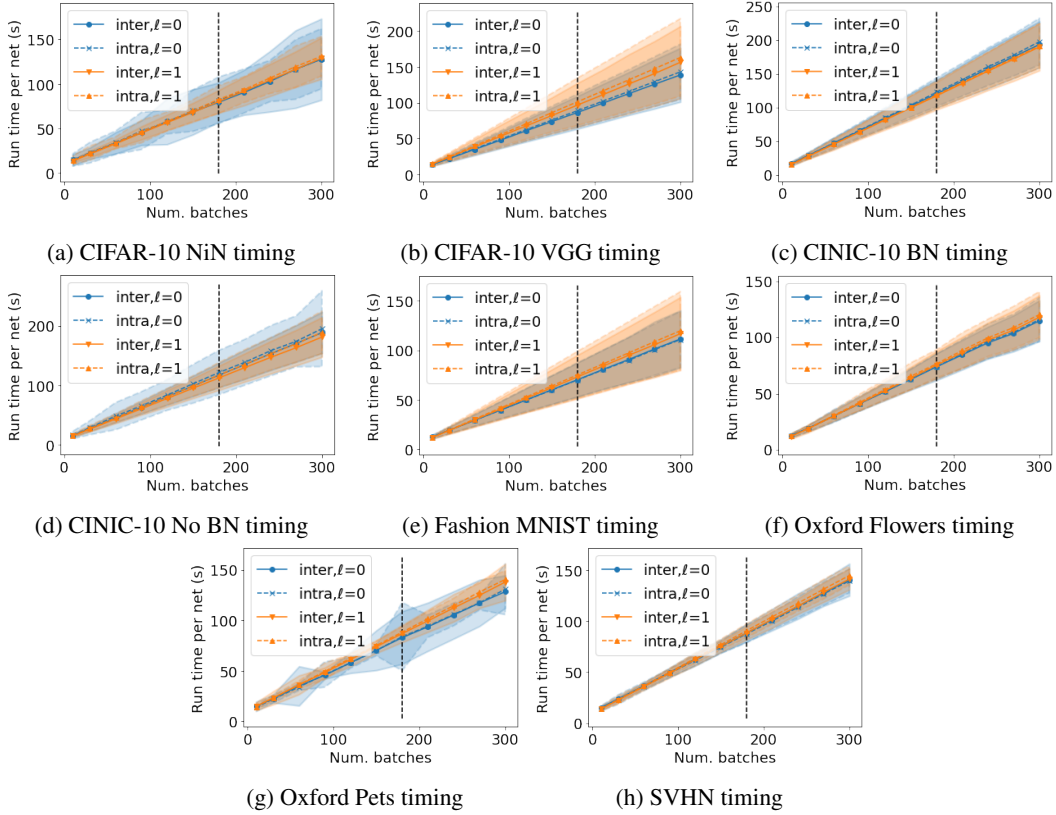


Figure 3: Perturbation response curve generation run times for each datasets on input layer and layer 1 ($\ell = 0$ and $\ell = 1$). Mean and std. dev. over 20 runs vs. number of batches - 180 batches used in results table (dotted line)

invariant to the test perturbation (as opposed to when they are all trained to be invariant, which can potentially be achieved across hyperparameters if the perturbations are used in training).

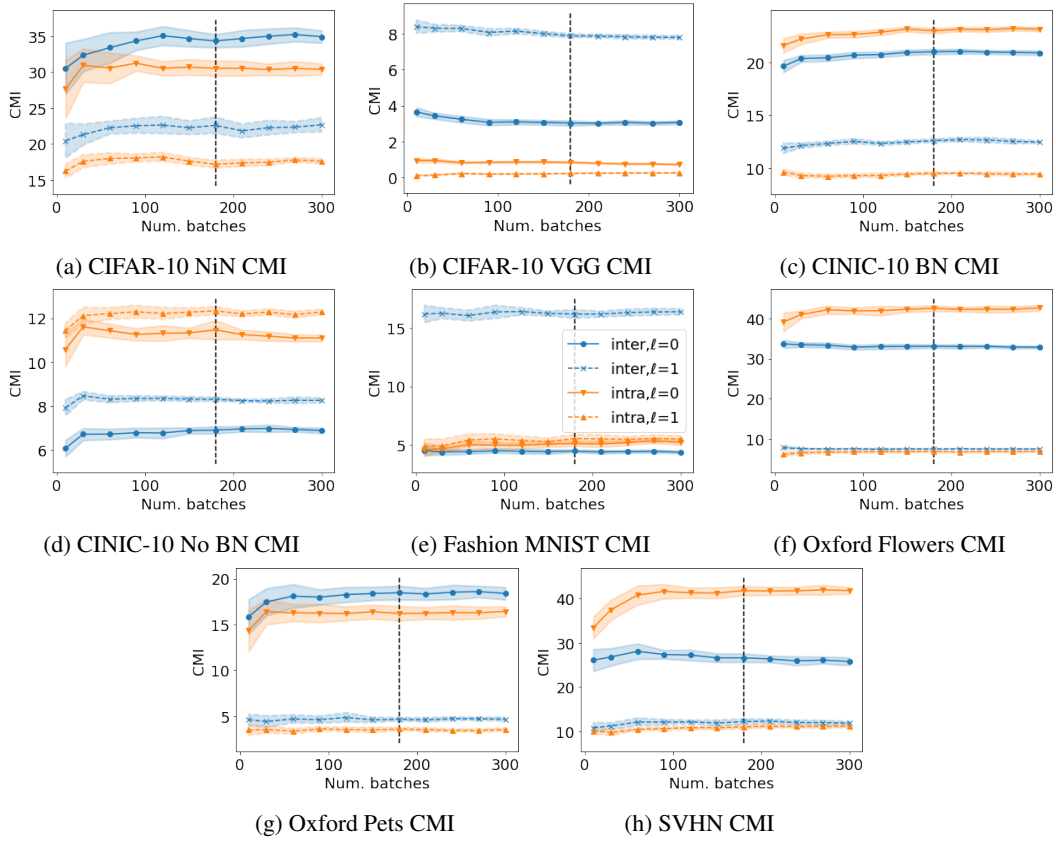


Figure 4: Conditional Mutual Information (CMI) score sensitivity results for all datasets on input layer and layer 1 ($\ell = 0$ and $\ell = 1$). Mean and std. dev. over 20 runs vs. number of batches - 180 batches used in results table (dotted line)

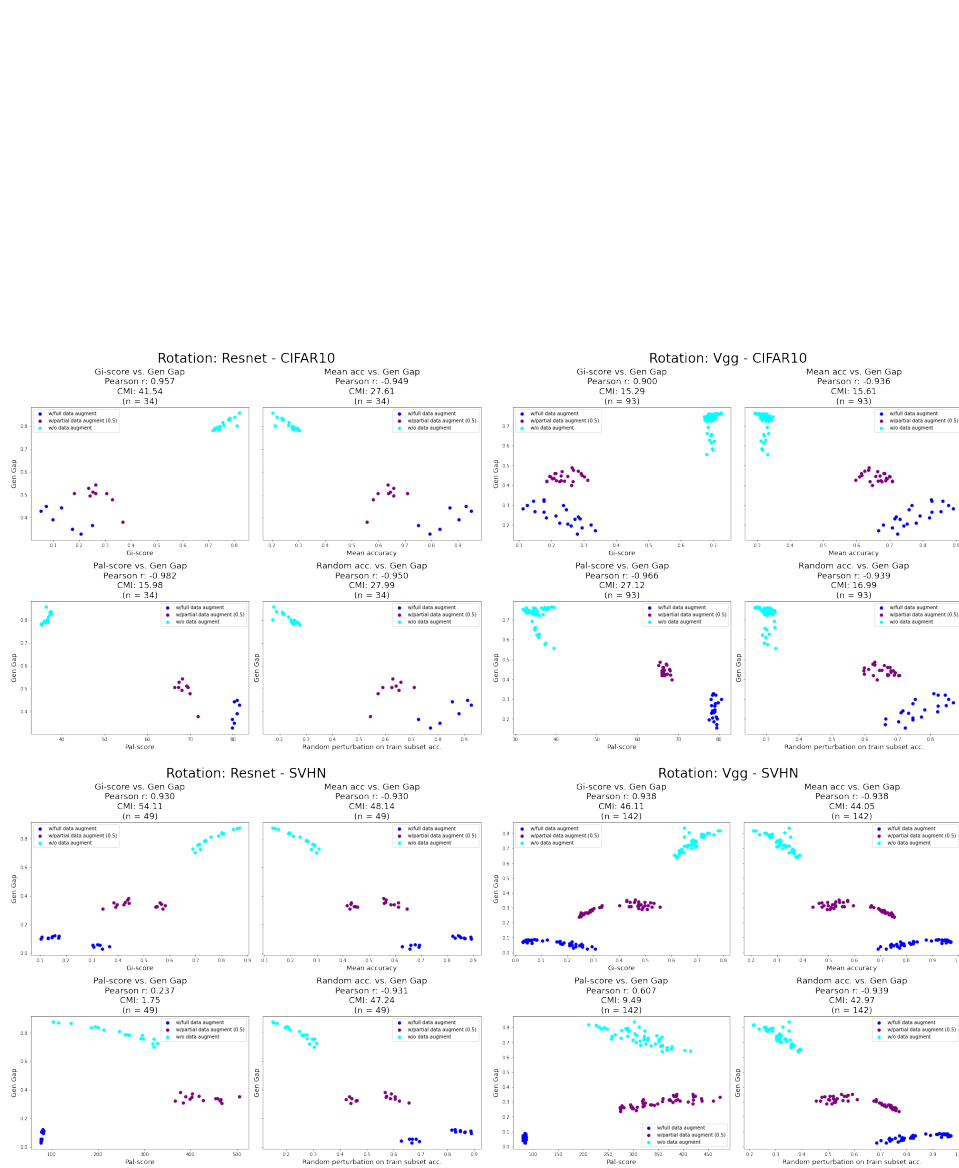


Figure 5: **Rotation:** Comparison of complexity measure and generalization gap for Resnet and VGG models trained on CIFAR-10 and SVHN to test how these measures predict generalization gap in the face of a rotation perturbation.

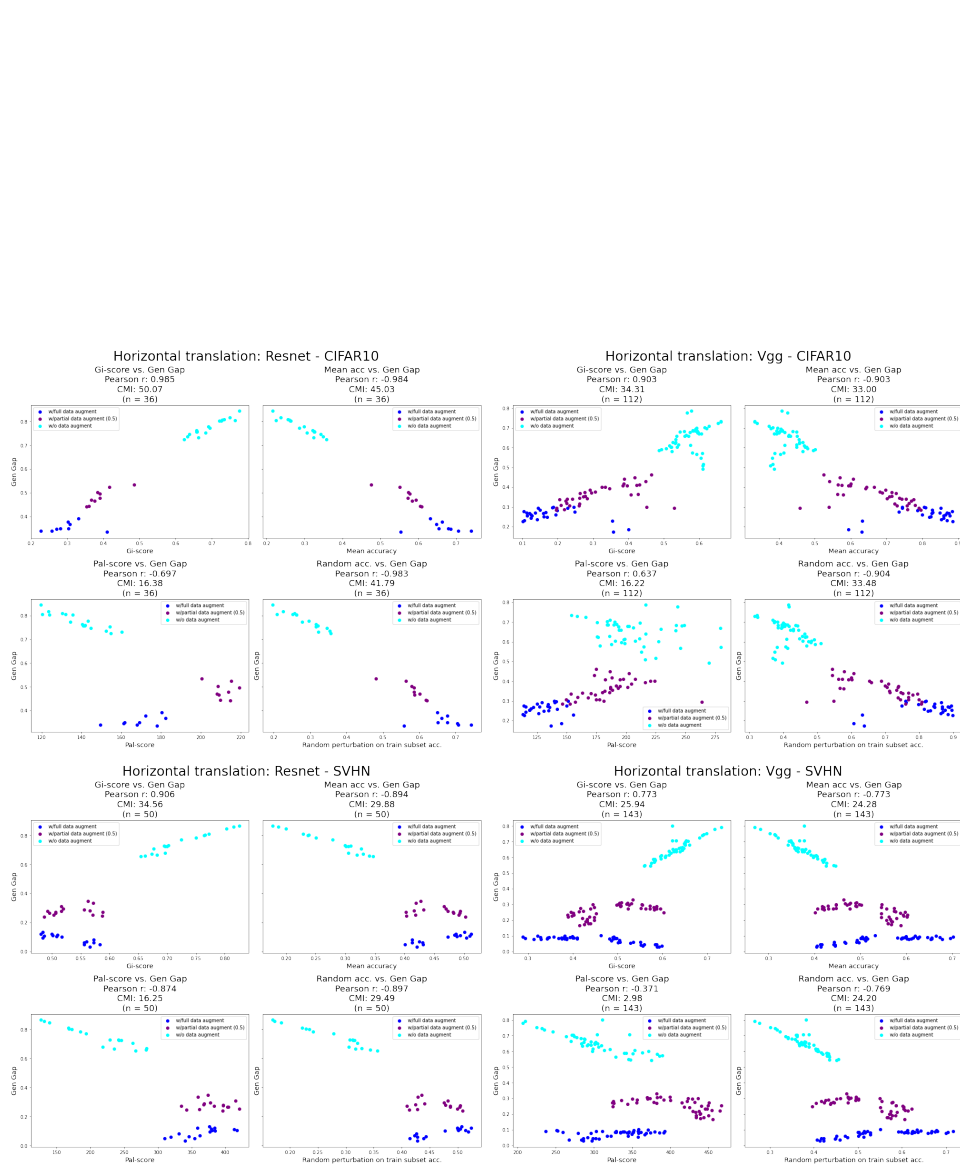


Figure 6: **Horizontal Translation:** Comparison of complexity measure and generalization gap for Resnet and VGG models trained on CIFAR-10 and SVHN to test how these measures predict generalization gap in the face of a horizontal translation perturbation.

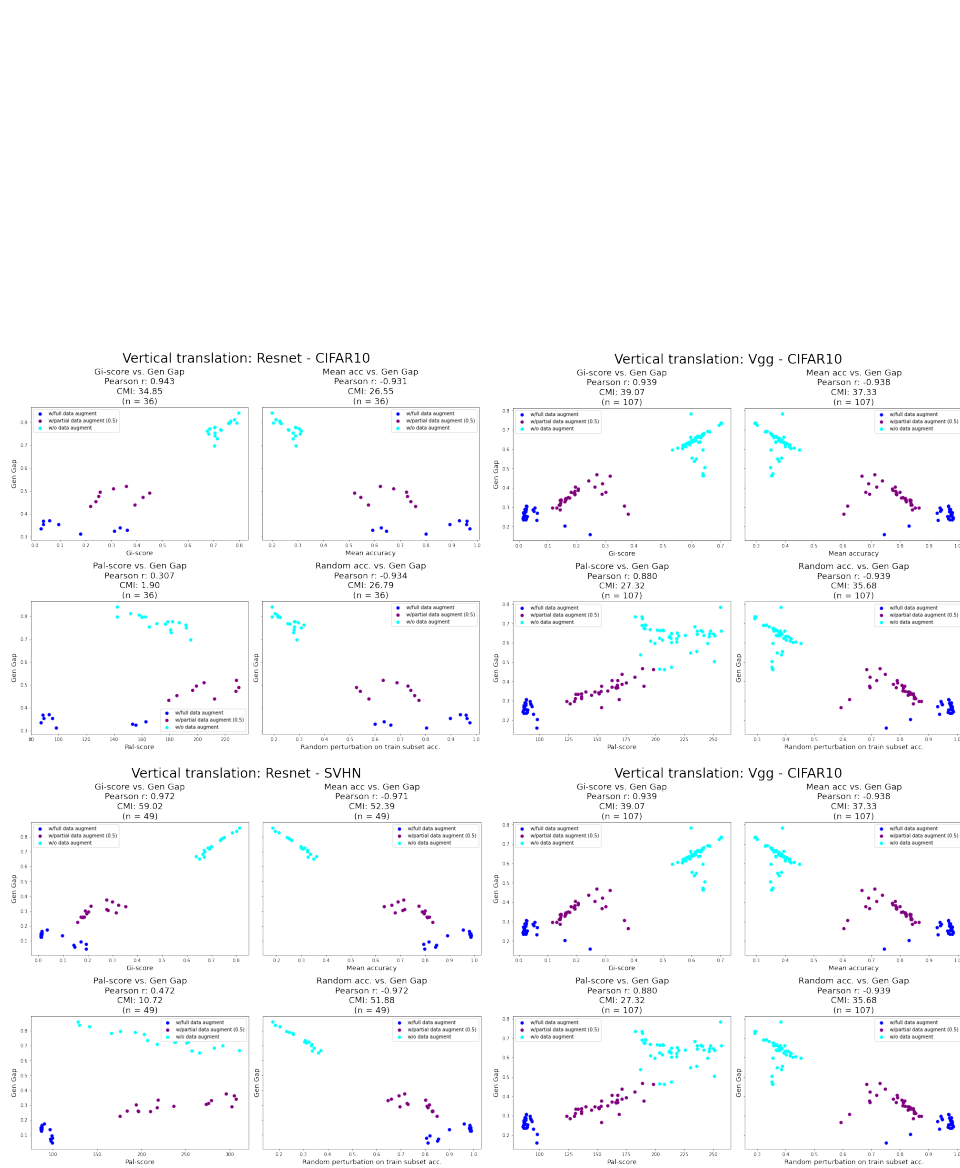


Figure 7: **Vertical Translation:** Comparison of complexity measure and generalization gap for Resnet and VGG models trained on CIFAR-10 and SVHN to test how these measures predict generalization gap in the face of a vertical translation perturbation.

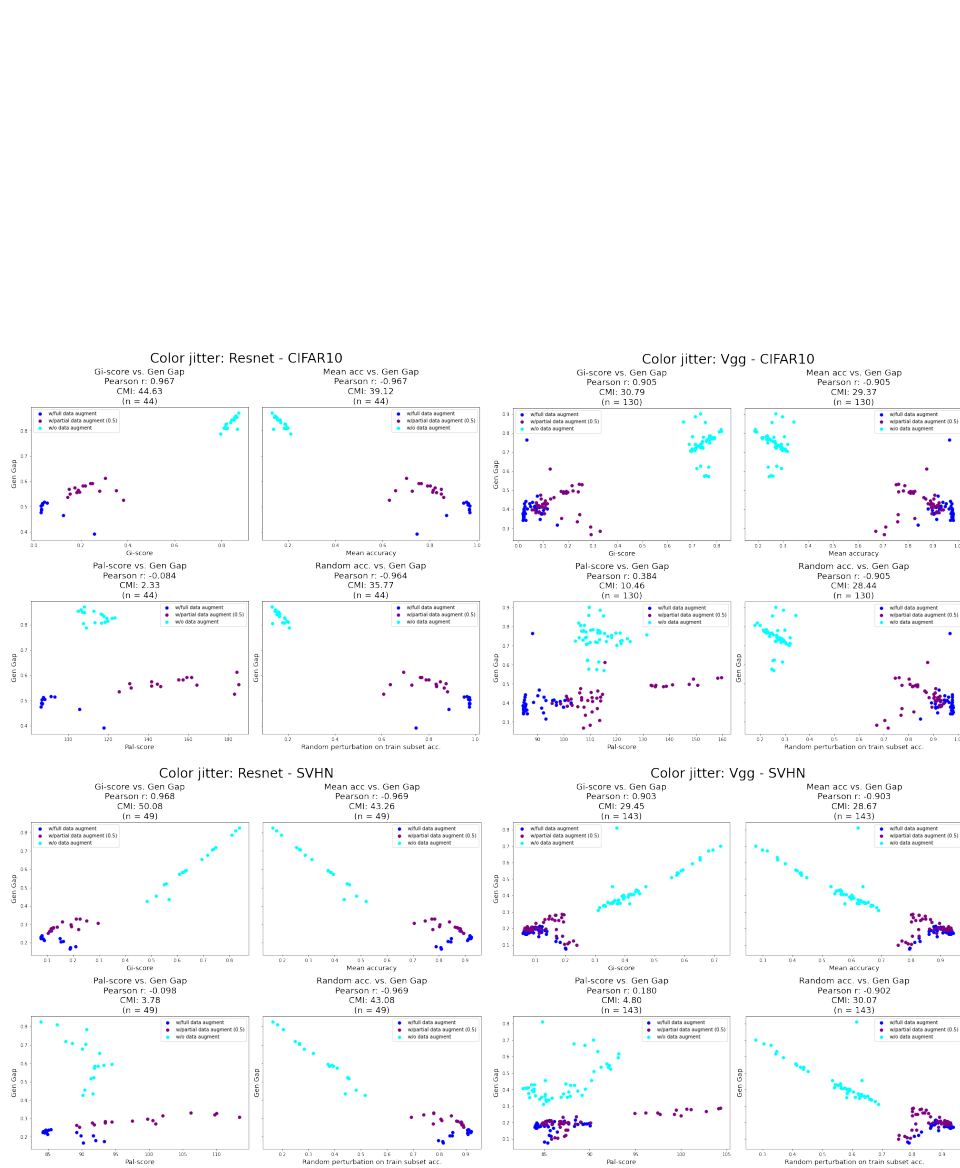


Figure 8: **Color-jittering**: Comparison of complexity measure and generalization gap for Resnet and VGG models trained on CIFAR-10 and SVHN to test how these measures predict generalization gap in the face of a color-jittering perturbation.